JACS
JOURNAL OF THE AMERICAN CHEMICAL SOCIETY

Subscriber access provided by ISTANBUL TEKNIK UNIV

Article

Determination of the Origin of Stereoselectivity in Multiple-Transition-State Reactions Using DFT Calculations: Enantioselective Synthesis of Homoallylic Alcohols from Aliphatic Methyl Ketones via an Auxiliary-Mediated Allylation

Lutz F. Tietze, Tom Kinzel, and Stefan Schmatz

J. Am. Chem. Soc., **2008**, 130 (13), 4386-4395 • DOI: 10.1021/ja078032a

Downloaded from http://pubs.acs.org on February 8, 2009

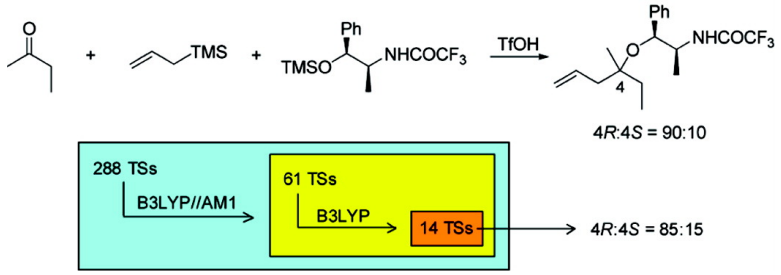

More About This Article

Additional resources and features associated with this article are available within the HTML version:

- Supporting Information
- Links to the 2 articles that cite this article, as of the time of this article download
- Access to high resolution figures
- Links to articles and content related to this article
- Copyright permission to reproduce figures and/or text from this article

View the Full Text HTML

ACS Publications
High quality. High impact.

Journal of the American Chemical Society is published by the American Chemical Society. 1155 Sixteenth Street N.W., Washington, DC 20036

J|A|C|S
ARTICLES
Published on Web 03/11/2008

Determination of the Origin of Stereoselectivity in Multiple-Transition-State Reactions Using DFT Calculations: Enantioselective Synthesis of Homoallylic Alcohols from Aliphatic Methyl Ketones via an Auxiliary-Mediated Allylation

Lutz F. Tietze,*,† Tom Kinzel,† and Stefan Schmatz‡

Institut für Organische und Biomolekulare Chemie, Georg-August-Universität Göttingen, Tammannstrasse 2, D-37077 Göttingen, Germany, and Institut für Physikalische Chemie, Georg-August-Universität Göttingen, Tammannstrasse 6, D-37077 Göttingen, Germany

Received October 19, 2007; E-mail: ltietze@gwdg.de

Abstract: Computational investigations on the highly stereoselective allylation of butanone in the presence of a chiral norpseudoephedrine-derived auxiliary have been performed. They suggest an S_N1-type mechanism via the attack of allyltrimethylsilane to an intermediately formed oxocarbenium ion. The identification of preferred transition states (TSs) leads to a straightforward rationalization of the observed selectivity which can be extended to analogues of the auxiliary. A screening process has been devised to select 61 potentially relevant TSs from a total of almost 300 theoretically possible TSs. Final results were obtained from gas-phase calculations employing the B3LYP/6-31+G(d) level of theory as well as in dichloromethane solution using the B3LYP/6-311++G(2d,p)//B3LYP/6-31+G(d) level of theory in combination with polarizable continuum model and the UAKS set of radii. The agreement of theoretically predicted and experimentally observed selectivities is very good in both cases. However, the relative energy differences for several relevant TSs differ significantly when going from gas phase to solution, thus illustrating the necessity of performing calculations in solution to draw correct conclusions.

1. Introduction

The enantioselective synthesis of tertiary homoallylic alcohols by allylation of aliphatic ketones using allylic metal reagents is a highly challenging task. Procedures which work well with aldehydes as well as aromatic and α,β-unsaturated ketones are considerably less selective when applied to aliphatic ketones.[1,2] On the other hand we have recently developed an auxiliary-mediated domino process[3] which leads to the corresponding homoallylic ether with excellent yields and selectivities using a mixture of the carbonyl compound, allyltrimethylsilane (**2**) and the norpseudoephedrine derivatives (*S*,*S*)-**3** or (*R*,*R*)-**3** in the presence of a catalyst.[4] For aldehydes, trimethylsilyl triflate, and for ketones, triflic acid (TfOH), are most suitable as catalysts. The ethers can easily be transformed into the corresponding homoallylic alcohols with >99% enantiomeric excess (ee) starting from aliphatic aldehydes and up to 98% ee using aliphatic methyl ketones. The reaction of butanone (**1**) as the most difficult ketone substrate with **2** and (*S*,*S*)-**3** in the presence of TfOH leads to the diastereomeric homoallylic ethers (4*R*)-**4** and (4*S*)-**4** in 90:10 ratio in 95% yield (Scheme 1).[4b] Larger

Scheme 1. Stereoselective Allylation of **1** in the Presence of the Norpseudoephedrine Derivative (*S*,*S*)-**3**

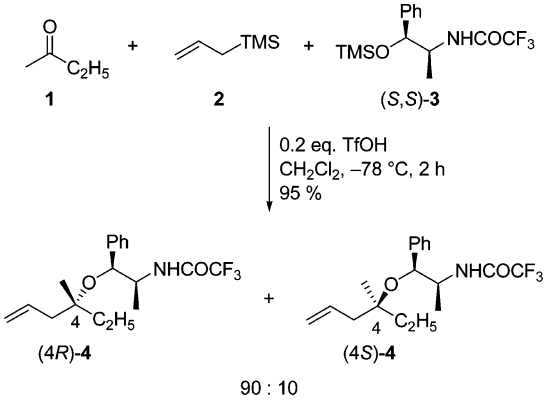

† Institut für Organische und Biomolekulare Chemie.
‡ Institut für Physikalische Chemie.

(1) (a) Denmark, S. E.; Fu, J. *Chem. Rev.* **2003**, *103*, 2763−2793. (b) Majetich, G. In *Organic Synthesis. Theory and Applications*; Hudlicky, T., Ed.; JAI Press, Greenwich, CT, 1989.

(2) (a) Wadamoto, M.; Yamamoto, H. *J. Am. Chem. Soc.* **2005**, *127*, 14556−14557. (b) Wada, R.; Oisaki, K.; Kanai, M.; Shibasaki, M. *J. Am. Chem. Soc.* **2004**, *126*, 8910−8911. (c) Huckins, J. R.; Rychnovsky, S. D. *J. Org. Chem.* **2003**, *68*, 10135−10145. (d) Waltz, K. M.; Gavenonis, J.; Walsh, P. J. *Angew. Chem.* **2002**, *114*, 3849−3852. Waltz, K. M.; Gavenonis, J.; Walsh, P. J. *Angew. Chem., Int. Ed.* **2002**, *41*, 3697−3699. (e) Nakamura, M.; Hirai, A.; Sogi, M.; Nakamura, E. *J. Am. Chem. Soc.* **1998**, *120*, 5846−5847. (f) Sames, D.; Liu, Y.; DeYoung, L.; Polt, R. *J. Org. Chem.* **1995**, *60*, 2153−2159. (g) Mekhalfia, A.; Markó, I. E. *Tetrahedron Lett.* **1991**, *32*, 4779−4782. (h) Soai, K.; Ishizaki, M. *J. Org. Chem.* **1986**, *51*, 3290−3295. (i) Roder, H.; Helmchen, G.; Peters, E.; Peters, K.; von Schnering, H. *Angew. Chem.* **1984**, *96*, 895−896. Roder, H.; Helmchen, G.; Peters, E.; Peters, K.; von Schnering, H. *Angew. Chem., Int. Ed.* **1984**, *23*, 898−899.

(3) (a) Tietze, L. F. *Chem. Rev.* **1996**, *96*, 115−136. (b) Tietze, L. F.; Brasche, G.; Gericke, K. *Domino Reactions in Organic Synthesis*, 1st ed.; Wiley VCH: Weinheim, Germany, 2006.

(4) (a) Tietze, L. F.; Dölle, A.; Schiemann, K. *Angew. Chem.* **1992**, *104*, 1366−1367. Tietze, L. F.; Dölle, A.; Schiemann, K. *Angew. Chem., Int. Ed. Engl.* **1992**, *31*, 1372−1373. (b) Tietze, L. F.; Schiemann, K.; Wegner, C. *J. Am. Chem. Soc.* **1995**, *117*, 5851−5852. (c) Tietze, L. F.; Wegner, C.; Wulff, C. *Synlett* **1996**, 471−472. (d) Tietze, L. F.; Wegner, C.; Wulff, C. *Eur. J. Org. Chem.* **1998**, 1639−1644. (e) Tietze, L. F.; Weigand, B.; Völkel, L.; Wulff, C.; Bittner, C. *Chem.—Eur. J.* **2001**, *7*, 161−168. (f) Tietze, L. F.; Völkel, L.; Wulff, C.; Weigand, B.; Bittner, C.; McGrath, P.; Johnson, K.; Schäfer, M. *Chem.—Eur. J.* **2001**, *7*, 1304−1308. (g) Tietze, L. F.; Hölsken, S.; Adrio, J.; Kinzel, T.; Wegner, C. *Synthesis* **2004**, *13*, 2236−2239.

10.1021/ja078032a CCC: $40.75 **© 2008 American Chemical Society**

Scheme 2. Possible Reaction Paths for the Multicomponent Allylation of Aliphatic Aldehydes and Methyl Ketones in the Presence of the Chiral Norpseudoephedrine-Derived Auxiliary (*S*,*S*)-**3**

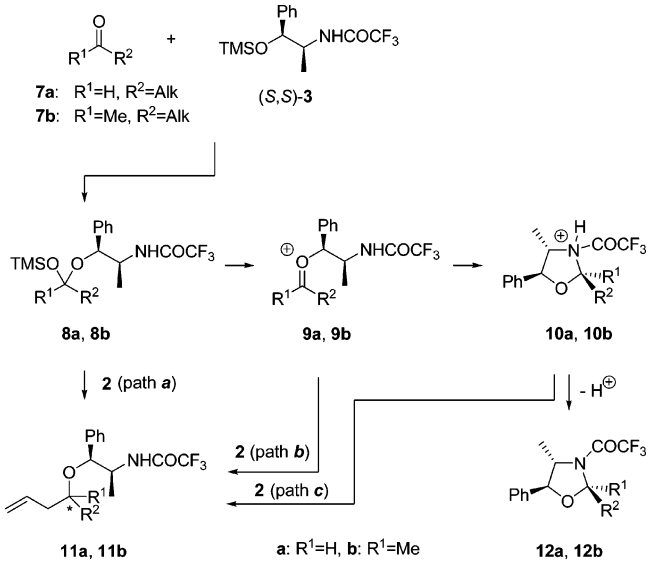

methyl ketones where the ethyl group is replaced by an isopropyl or an *tert*-butyl group yield improved selectivities of >24:1 and 10:1, respectively.

In the process of the development of simplified analogues of **3** for the allylation of ketones,[4c] we have found that the methyl group in **3** is not necessary for a selective allylation (Figure 1). Thus, with (*S*)-**5** in which the methyl group is replaced by a hydrogen atom, almost the same selectivity as with (*S*,*S*)-**3** is found, while by inverting the stereochemistry at C-2 of **3** a selectivity of 87:11 was observed. On the other hand, replacing the phenyl group in (*S*)-**5** with a naphthalene group enhances the selectivity.

Determining the origin of stereoselectivity of any reaction comprises two parts: First, a sound mechanistic proposal must be developed to give information on the intermediates and the elementary steps connecting them, and second, the transition states (TSs) of the stereoselective step that lead to the product isomers must be identified.

Here we describe the computational elucidation of the origin of the stereoselectivity of the allylation of **1** in the presence of (*S*,*S*)-**3**. The results also lead to a rationalization of the divergent selectivities when (*S*)-**5**, (*S*,*R*)-**3**, and (*S*)-**6** are employed as chiral auxiliaries. We realize that the differences in selectivity with these auxiliaries are rather small; however, the fact that this rationalization is easily possible constitutes a verification of the identified TS structures.

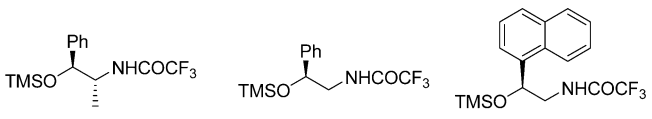

Figure 1. Analogues of (*S*,*S*)-**3** and the induced selectivity in allylations of **1** under reaction conditions identical to those displayed in Scheme 1.

Scheme 2 shows the possible mechanistic pathways for the multicomponent allylation of aliphatic aldehydes and ketones in the presence of (*S*,*S*)-**3**: First, the reaction of silyl ether **3** and carbonyl compound **7** gives the mixed acetal **8**. The homoallylic ether **11** as the final product may then be formed by a direct S_N2 reaction at the acetal (path a), or via formal elimination of $TMSO^-$ and subsequent nucleophilic attack of the silane **2** to the oxocarbenium ion **9** (path b), or via an intermediate of type **10** (path c).

In aldehyde allylations with **3**, the oxazolidine **12a** was formed as a byproduct and became the main product when the reaction temperature was raised. In situ ^{13}C NMR experiments showed the intermediate formation of diastereomerically pure **10a** which was intercepted by **2**, allowing a straightforward explanation for both the direction and the high magnitude of the selectivity in the formation of **11a**.[5]

In contrast to the aldehyde allylations, no corresponding heterocyclic byproduct **12b** was found when aliphatic methyl ketones were employed as substrates. In in situ ^{13}C NMR experiments, only the signals of the mixed acetal **8b** could be detected.[6] In addition, an opposite induced stereoselectivity is found when going from aldehydes to ketones, assuming that the methyl group and the hydrogen atom, respectively, are the smallest substituent at the carbonyl moiety. Therefore, the reaction path c via formation of **10b** can be ruled out.

With a stereochemical experiment employing the chiral silyl ether TMSO−*CHPhMe, it was shown that aldehyde allylations do not proceed via path a.[7] For ketone allylation, path a becomes even less likely since S_N2 reactions at **8** with R^1 = Me should be less favored than those in the case of R^1 = H.

Therefore, we propose that the allylation of **1** with (*S*,*S*)-**3** proceeds in an S_N1-type fashion via path b. This assumption is further substantiated by our earlier study[8] where it was shown that the syn/anti diastereoselectivity in crotylation reactions of ketones and aldehydes in the presence of methoxytrimethylsilane could be rationalized by the addition of crotyltrimethylsilane to an *O*-methyl oxocarbenium ion.

The results of a number of experimental and computational investigations on allylation reactions of Lewis-acid-activated aldehydes with allyl silanes draw a picture of the TS structures involved. Conformational analysis of carboxenium ions and investigations on attack trajectories have been performed by Houk et al., but without determining TS geometries.[9] Experimental evidence comes from strained, intramolecular systems,[10] while computational investigations have been performed only for simplified systems.[11] One TS for the attack of allyl trimethylsilane to protonated acetaldehyde has been identified.[12]

By a systematic study of all possible TSs for the addition of **2** to **13** to form an intermediate carbenium ion **14** (Scheme 3), we identified those which are responsible for the preferential formation of (4*R*)-**4**.

2. Transition-State Nomenclature

In the following, a TS nomenclature is introduced which is based on Newman projections such as those shown in Chart 1

(5) Tietze, L. F.; Wulff, C.; Wegner, C.; Schuffenhauer, A.; Schiemann, K. *J. Am. Chem. Soc.* **1998**, *120*, 4276−4280.
(6) Adrio, J. Diploma Thesis, Universität Göttingen, Germany, 2002.
(7) Manju, K.; Trehan, S. *Chem. Commun.* **1999**, 1929−1930.
(8) Tietze, L. F.; Kinzel, T.; Schmatz, S. *J. Am. Chem. Soc.* **2006**, *128*, 11483−11495.
(9) (a) Paddon-Row, M. N.; Rondan, N. G.; Houk, K. N. *J. Am. Chem. Soc.* **1982**, *104*, 7162−7166. (b) Broeker, J. L.; Hoffmann, R. W.; Houk, K. N. *J. Am. Chem. Soc.* **1991**, *113*, 5006−5017.
(10) (a) Denmark, S. E.; Weber, E. J. *J. Am. Chem. Soc.* **1984**, *106*, 7970−7971. (b) Denmark, S. E.; Willson, T. M. *J. Am. Chem. Soc.* **1989**, *111*, 3475−3476. (c) Denmark, S. E.; Almstead, N. G. *J. Org. Chem.* **1994**, *59*, 5130−5132. (d) Denmark, S. E.; Hosoi, H. *J. Org. Chem.* **1994**, *59*, 5133−5135.
(11) Bottoni, A; Costa, A. L.; Di Tommaso, D.; Rossi, I.; Tagliavini, E. *J. Am. Chem. Soc.* **1997**, *119*, 12131−12135.
(12) Mayer, P. S.; Morton, T. H. *J. Am. Chem. Soc.* **2002**, *124*, 12928−12929.

Chart 1. 24 General Attack Trajectories for the Addition of **2** to **13** (R = $CH(CH_3)-NHCOCF_3$, R* = $CHPh-CH(CH_3)-NHCOCF_3$)

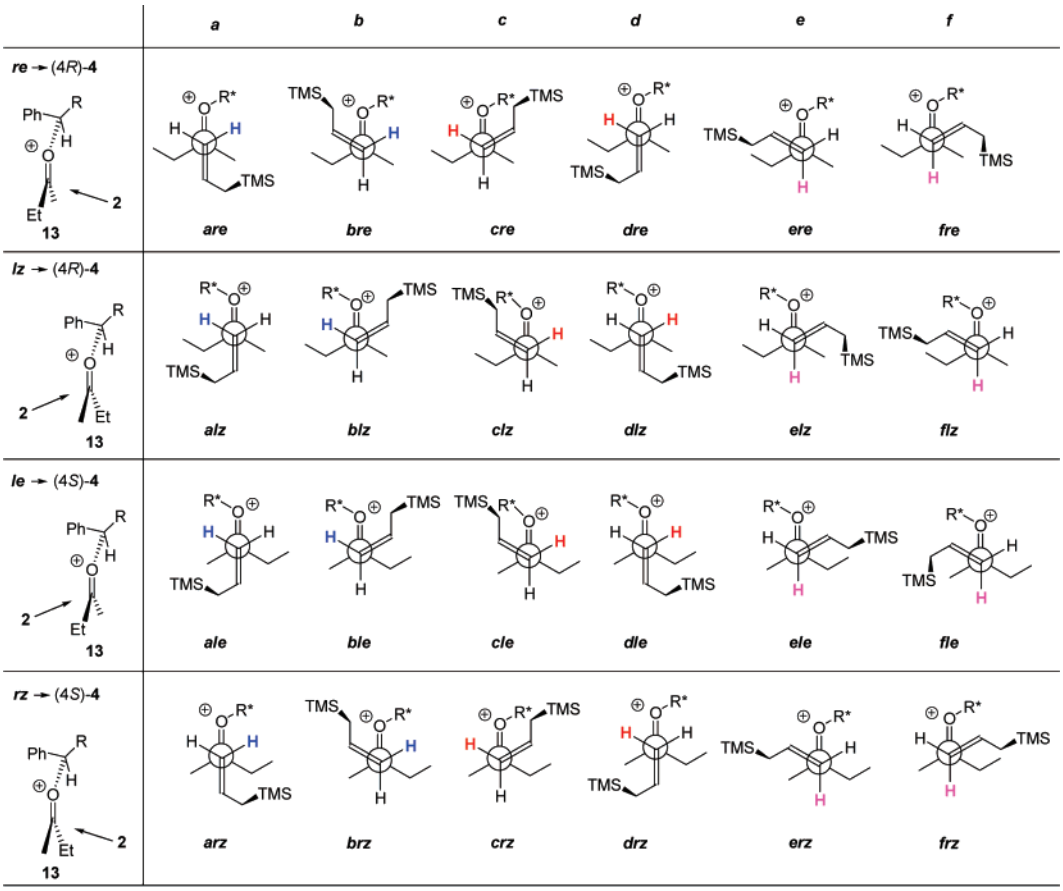

Scheme 3. Proposed Stereogenic Step and Subsequent Double-Bond Regeneration to Form Homoallylic Ether **4** from Oxocarbenium Ion **13** and **2**

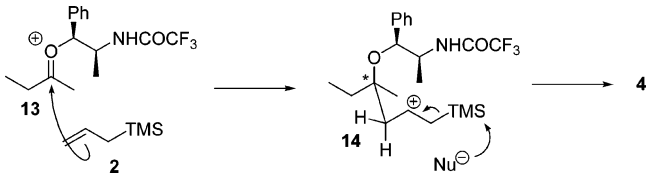

with the attacking silane **2** in front and the attacked oxocarbenium ion **13** in the back. The basis for these TS conformations is the fact that allylsilanes attack carboxenium ions via open TSs.[13]

There are four classes of attack depending on the double-bond geometry and the approached face of **13** that decide upon the configuration of the newly formed stereogenic center: In the chosen projection, the chiral unit R* either points to the right-hand side (denoted by ***r***) or to the left-hand side (denoted by ***l***). In ***l***-TSs, **2** approaches **13** to the face where the phenyl group resides, while in ***r***-TSs, **2** attacks the opposite face. The oxocarbenium double bond may be E- or Z-configured, denoted by ***e*** and ***z***, respectively. The combinations ***re*** and ***lz*** thus describe nucleophilic attack to the *Si* face of **13** to yield the (4*R*)-configured product **4**, while ***le*** and ***rz*** combinations give (4*S*)-**4** via attack to the *Re* face.

Additionally, there are six orientations of the attacking silane **2** in relation to **13**, denoted by ***a***−***f***. In trajectories ***a*** and ***b***, the double-bond hydrogen cis to the CH_2TMS group in **2** points to the same direction as R*, while in trajectories ***c*** and ***d***, it points away from it. Finally, in ***e*** and ***f*** trajectories the cis hydrogen lies between the methyl and ethyl groups of **13**. Starting from attack trajectory ***a***, counterclockwise rotation around the C···C axis leads to trajectories ***c*** and ***e***, and in the same way trajectories ***b***, ***d***, and ***f*** are connected with each other.

Chart 1 shows the 24 general attack trajectories resulting from these three conformational degrees of freedom.

In addition, three degrees of freedom in **13** need to be taken into account: First, the methyl moiety of the ethyl group may point backward (away from **2**), denoted by ***b***, or downward, denoted by ***d*** (Figure 2).

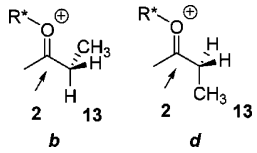

Figure 2. Conformational degrees of freedom in TSs caused by different orientations of the ethyl group (R* = $CHPh-CH(CH_3)-NHCOCF_3$).

Second, possible conformations in the auxiliary side chain are shown in Chart 2 where there are three minima ***1***−***3*** differing in the torsional angle Ph−C−C−N. Third, the hydrogen atoms at the nitrogen and the adjacent carbon atom adopt either synperiplanar (***s***) or antiperiplanar orientation (***a***).

The combinations of the 24 basic attack trajectories with the three additional degrees of freedom lead to a total of 288 TS conformations ($6_{a-f} \times 2_{r,l} \times 2_{e,z} \times 2_{b,d} \times 3_{1-3} \times 2_{a,s} = 288$).

(13) Denmark, S. E.; Weber, E. J. *Helv. Chim. Acta* **1983**, *159*, 1655−1660.

Chart 2. Auxiliary Side Chain Conformations in **13**. Here, ***s*** and ***a*** Labels Are Given to Synperiplanar or Antiperiplanar Orientations of the Shaded Hydrogen Atoms, Respectively

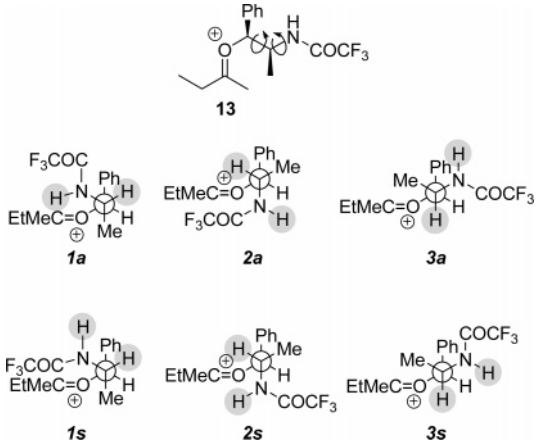

In the following, TSs are denoted by a six-character code, e.g., ***are-b3a*** or ***flz-d2s***, using the nomenclature introduced above.

3. Computational Strategy

All calculations reported in this work were performed with the *Gaussian 03* program package.[14] The B3LYP[15] density functional with the 6-31+G(d) basis set was employed for TS geometry optimizations and frequency calculations in the gas phase (B3LYP-GP). In order to include effects exerted by the solvent dichloromethane, the same level of theory was used in combination with the polarizable continuum model (PCM)[16] method and the UAKS set of radii (B3LYP-PCM). In all calculations, the temperature was set to the experimental value (T = 195 K). Obtained TS geometries were validated by inspection of the Hessian matrices.

The B3LYP-PCM results were further refined by single-point energy determination using the B3LYP/6-311++G(2d,p)/PCM/UAKS (B3LYP-PCM-large) level of theory. Here, the free-energy values G were obtained by adding the correction terms G_{korr}, obtained via B3LYP-PCM frequency calculations, to the B3LYP-PCM-large single-point energy that comprises the electronic potential and the solvation free energy $E_0 + \Delta G_{\mathrm{solv}}$ (eq 1).

$$G = \underbrace{E_0 + \Delta G_{\mathrm{solv}}}_{\text{B3LYP-PCM-large//B3LYP-PCM}} + \underbrace{G_{\mathrm{korr}}}_{\text{B3LYP-PCM}} \qquad (1)$$

It was found that $G^{\ddagger}_{\mathrm{rel}}$ values obtained are almost identical when using either the B3LYP-PCM or the B3LYP-PCM-large//B3LYP-PCM method. This observation indicates that the basis set superposition error (BSSE) is a systematic error that vanishes when determining *relative* energies.

The activation energy $\Delta G^{\ddagger}$ for the stereogenic step was determined via B3LYP-PCM-large//B3LYP-PCM calculations of the ground states of **2** and **13** in comparison with the lowest-energy TSs. In contrast to the determination of selectivity, the single-point calculation with a large basis set is necessary for the determination of $\Delta G^{\ddagger}$ in order to reduce the BSSE.

The induced diastereoselectivity for the addition of allyltrimethylsilane (**2**) to oxocarbenium ion **13** has been determined computationally employing reaction rate coefficients calculated according to transition-state theory. The contribution of a single TS to the overall rate of product formation c_{TS} is given by eq 2

$$c_{\mathrm{TS},i} = \exp\left(-\frac{G^{\ddagger}_{\mathrm{rel},i}(T)}{RT}\right) \Bigg/ \sum_{j\in\{\mathrm{TS_R}\cup\mathrm{TS_S}\}} \exp\left(-\frac{G^{\ddagger}_{\mathrm{rel},j}(T)}{RT}\right) \times 100\% \qquad (2)$$

with T = 195 K. $G^{\ddagger}_{\mathrm{rel},j}$ denotes the free energy difference between the jth TS and the TS with lowest free energy. $\mathrm{TS_R}$ and $\mathrm{TS_S}$ denote index sets of the respective classes of TSs. The product ratio of (4*R*)-**4** is then obtained by adding the c_{TS} values of all TSs that give the *R*-configured product

$$\mathrm{PR_R} = \sum_{i\in\{\mathrm{TS_R}\}} c_{\mathrm{TS},i} \qquad (3)$$

According to eq 2, only TSs with a relative free-energy difference to the lowest-energy TS of $G^{\ddagger}_{\mathrm{rel}} \leq 6.0$ kJ mol^{-1} (in the following, termed "relevant TSs") may contribute more than 2% to the product ratio at T = 195 K in the limiting case of only one lower-energy TS. However, both in gas phase and in solution, more than two relevant TSs could be identified. Consequently, higher-energy TSs can be neglected without loss of accuracy.

Recently, several reports have shown that density functional theory (DFT) methods exhibit large errors in the prediction of isomerization energies of constitutional isomers of hydrocarbons, and the authors discourage the use of such methods, especially B3LYP, for the study of large systems.[17] The use of the B3LYP functional in this study is however justified since systematic errors cancel out each other for two reasons: First, the prediction of selectivity is based on *relative* energy differences of TSs which only differ in their conformation, but not in their constitution. Second, it is rather unlikely that the remaining error accumulates when calculating the selectivity from more than two relevant TSs according to eqs 2 and 3. In addition, we have shown that the selectivities of a series of similar, albeit simpler reactions could be explained with B3LYP-calculated TSs.[8]

Due to the large number of possible TSs, a screening process has been developed to select potentially relevant TS before performing time-consuming calculations with the B3LYP-GP or B3LYP-PCM methods: First, 264 TS geometries were located employing the semiempirical AM1 method. (As impossible constraints are imposed by some combinations of the geometrical parameters of the conformational degrees of freedoms, 24 TSs could not be found.) Then, B3LYP-GP//AM1 single-point calculations yielded a list of relative TS energies from which all TSs with a relative energy $E^{\ddagger}_{\mathrm{rel}} \leq 15.0$ kJ mol^{-1} were selected (37 TSs). Another 10 TSs with $E^{\ddagger}_{\mathrm{rel}} <$ 20 kJ

(14) Frisch, M. J. et. al. *Gaussian 03*, revision B.04; Gaussian, Inc.: Wallingford, CT, 2004.

(15) (a) Becke, A. D., *Phys. Rev. A: At., Mol., Opt. Phys.* **1988**, *38*, 3098−3100. (b) Lee, C.; Yang, W.; Parr, R. G. *Phys. Rev. B: Condens. Matter Mater. Phys.* **1988**, *37*, 785−789. (c) Becke, A. D. *J. Chem. Phys.* **1993**, *98*, 5648−5652.

(16) (a) Mennuci, B.; Cammi, R.; Tomasi, J. *J. Chem. Phys.* **1999**, *110*, 6858−6870. (b) Cossi, M.; Scalmani, G.; Rega, N.; Barone, V. *J. Chem. Phys.* **2002**, *117*, 43−54.

(17) (a) Schreiner, P. R. *Angew. Chem.* **2007**, *119*, 4295−4297. Schreiner, P. R. *Angew. Chem., Int. Ed.* **2007**, *46*, 4217−4219. (b) Grimme, S.; Steinmetz, M.; Korth, M. *J. Org. Chem.* **2007**, *72*, 2118−2126. (c) Grimme, S. *Angew. Chem., Int. Ed.* **2006**, *118*, 4571−4575. Grimme, S. *Angew. Chem., Int. Ed.* **2006**, *45*, 4460−4464. (d) Schreiner, P. R.; Fokin, A. A.; Pascal, R. A., Jr.; de Meijere, A. *Org. Lett.* **2006**, *8*, 3635−3638. (e) Wodrich, M. D.; Corminboeuf, C.; Schleyer, R. *Org. Lett.* **2006**, *8*, 3631−3634.

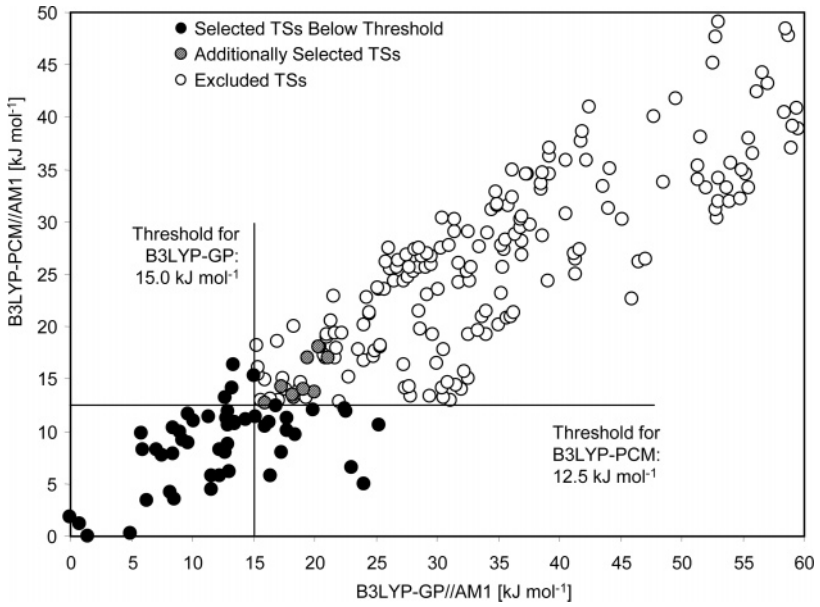

Figure 3. Selected TSs from B3LYP//AM1 single-point calculations.

mol^{-1} were included in the TS set for additional verification purposes. Similarly, B3LYP-PCM//AM1 calculations allowed us to select 48 TSs with $E_{rel}^{\ddagger} \leq 12.5$ kJ mol^{-1}. All final DFT calculations were then performed with the combined set of 61 TSs (Figure 3).

The aim of the screening process was to select a subset of TS geometries that contains *all* relevant TSs. Thus, the described procedure is only applicable when three criteria are met: First, every TS geometry identified with AM1 must unequivocally correspond to one TS geometry at the DFT level. Second, since the selection is based on *relative* energy differences, the errors of the TS geometries that are introduced by the approximations of the semiempirical method must be *uniformly* systematic in nature. Third, the threshold for selection must be chosen large enough not to miss any relevant TSs and to account for changes in relative energy when comparing potential energy $E_{rel}^{\ddagger}$ instead of free energy $G_{rel}^{\ddagger}$. To illustrate that the first criterion is met, we have performed relaxed potential energy scans starting from TS ***ele-b3a*** where the torsional angle γ = (C═C···C═O) is fixed to multiples of 30°, thus including TSs ***cle-b3a*** and ***ale-b3a***. Geometry optimizations to first-order saddle points were then carried out on each of the resulting 12 points (Figure 4).

Curves 1, 2, and 4 represent the energy surface on which the geometry optimization was carried out for each point at the AM1, B3LYP-GP, and B3LYP-PCM levels of theory, respectively. For comparison, curves 3 and 5 show the approximated B3LYP energy surface obtained via B3LYP//AM1 single-point calculations. For each curve, the point with lowest energy was arbitrarily set to zero. While there are certainly differences in the detail around the minima, the overall picture clearly shows that each AM1-TS corresponds to one TS with either B3LYP method. In addition, Figure 4 shows that B3LYP relative TS energies $E_{rel}^{\ddagger}$ are reasonably better reproduced by B3LYP//AM1 than by using AM1 directly.

The second criterion was shown to be fulfilled by comparison of the B3LYP//AM1 single-point energy (including ΔG_{solv} for B3LYP-PCM) with the B3LYP potential energy obtained after B3LYP geometry optimization. This energy difference, which

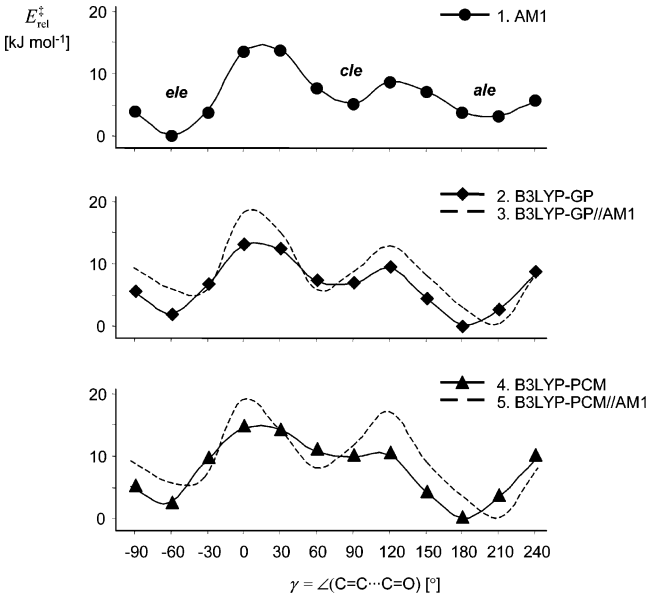

Figure 4. Relaxed potential energy surface scans by variation of γ = ∠(C═C···C═O). Every point represents a C−C bond-forming TS with fixed γ value. Minima of the 1D profiles correspond to TSs (first-order saddle points), and maxima represent second-order saddle points.

is a measure for the difference in the TS geometry predicted by AM1 and B3LYP, was found to be about 85−90 kJ mol^{-1}. Despite this large difference, the standard deviation of the energy difference for the chosen set of 61 TSs is only 2.5 kJ mol^{-1} for both the B3LYP-GP and the B3LYP-PCM methods. Additionally, we did not observe any dependence of this energy difference on $E_{rel}^{\ddagger}$, thus justifying the decision to exclude higher-energy TSs.

Figure 5 compares the B3LYP//AM1 results with the final B3LYP results. The maximum negative deviation (meaning that the final B3LYP relative free energy is lower than the relative energy obtained via B3LYP//AM1) between $E_{rel}^{\ddagger}$ from B3LYP-GP//AM1 and $G_{rel}^{\ddagger}$ from B3LYP-GP is −4.2 kJ mol^{-1}. From the figure, it is obvious that the correlation between B3LYP-PCM and B3LYP-PCM//AM1 is less consistent than that for

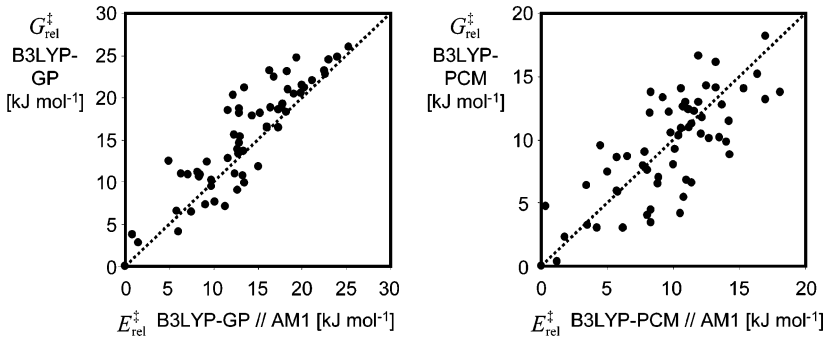

Figure 5. Comparison between $E^{\ddagger}_{rel}$ from B3LYP//AM1 single-point calculations with $G^{\ddagger}_{rel}$ values obtained by B3LYP geometry optimization and frequency calculation. The dotted lines show a hypothetical 1:1 correlation between the energy values.

Chart 3. Selected Important TSs As Calculated via B3LYP-GP[a]

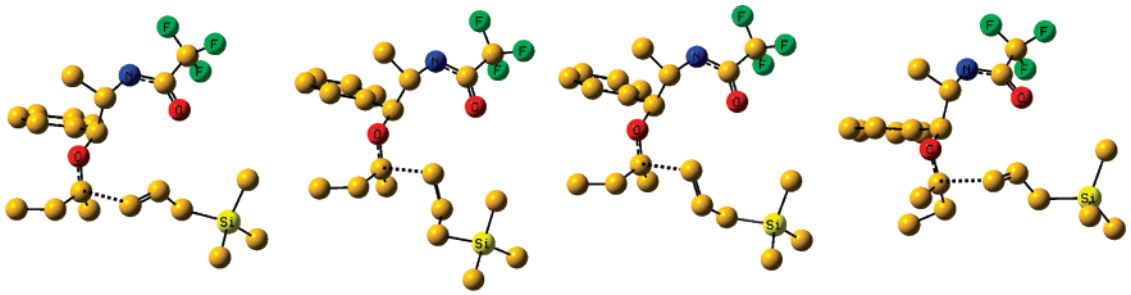

[a] Hydrogen atoms are omitted for clarity.

Table 1. Important TSs Obtained from B3LYP-GP Calculations

TS[a]	$G^{\ddagger}_{rel}$ (kJ mol^{-1})	c_{TS} (%)[b]	
fre-b3a (*R*)	0.0	69.1	
dre-b3a (*R*)	2.8	12.0	
are-b3a (*R*)	3.7	6.8	
fre-d3a (*R*)	4.1	5.5	(4*R*)-**4**:
bre-b3a (*R*)	6.4	1.3	97%
ere-b3a (*R*)	7.1	0.8	
are-d3a (*R*)	9.0	0.3	
cre-b3a (*R*)	9.6	0.2	
frz-d3a (*S*)	6.6	1.2	
frz-b3a (*S*)	7.3	0.8	(4*S*)-**4**:
arz-b3a (*S*)	7.6	0.6	3%
drz-b3a (*S*)	9.5	0.2	
ale-b3a (*S*)	9.9	0.2	

[a] The induced product stereochemistry at the C-4 position of homoallylic ether **4** is given in parentheses. [b] c_{TS} = transition-state contribution, as calculated according eq 2. For the calculation of c_{TS}, only the TSs in the table were considered.

the gas-phase calculations, which is due to the fact that the AM1 TS geometries were determined without inclusion of solvent effects. However, the maximum negative deviation is still limited to only −6.4 kJ mol^{-1}.

4. Results and Discussion

Gas-Phase Results. Four TSs with $G^{\ddagger}_{rel}$ < 6.0 kJ mol^{-1} were found which all lead to the formation of the (4*R*)-configured homoallylic ether **4**. Table 1 lists all TSs up to 10.0 kJ mol^{-1}, the $G^{\ddagger}_{rel}$ values of which predict a 97:3 ratio in favor of (4*R*)-**4**, which is in reasonable agreement with the experimental result (90:10).

The auxiliary side chain in all important TSs exclusively adopts conformation ***3a*** (Chart 2). The formation of the main isomer can be traced back to the attack of **2** to the *Si* face of the E-configured oxocarbenium ion **13**. The minor isomer is formed by attack to the *Re* face of the Z-configured ion **13**. Thus, the attack of **2** to **13** in important TSs always occurs from the face opposite to the phenyl group of the auxiliary. The first TS with attack to the face where the phenyl group is located, TS ***ale-b3a***, has a value of $G^{\ddagger}_{rel}$ = 9.9 kJ mol^{-1}, and its contribution to product formation is negligibly small. Chart 3 shows TSs ***fre-b3a***, ***dre-b3a***, ***are-b3a***, and ***frz-b3a***.

The B3LYP-GP results explain the experimental observation that larger methyl ketones give better selectivities, since the energy difference between E- and Z-configured oxocarbenium ions becomes larger. However, the selectivities with the auxiliary analogues (*S*)-**5**, (*S*,*R*)-**3**, and (*S*)-**6** cannot be explained: Assuming that the position of the trifluoroacetamide moiety in side chain conformation ***3a*** remains the same, exchange of the methyl group by a hydrogen atom (in the case of (*S*)-**5**) would not change $G^{\ddagger}_{rel}$ values at all. Inverting the stereochemistry at this center (for (*S*,*R*)-**3**) leads to conformations where the methyl group points toward the approaching allyl silane. While this effect might induce higher activation energies and a smaller reaction rate, it does not change the $G^{\ddagger}_{rel}$ values because it applies uniformly to all relevant TSs. Finally, B3LYP-GP results predict the phenyl group to be large enough to absolutely prevent attack to its face, so that replacement by the larger naphthalene group (for (*S*)-**6**) should not lead to improved selectivity.

From this reasoning, we must conclude that although B3LYP-GP delivers a good prediction of the isomer ratio, it does so coincidentally without having identified the correct TSs.

Calculations Including Solvent Effects. Because of the unexplicable experimental evidence and because of the overestimated magnitude of selectivity in gas-phase calculations, we have decided to include the effects exerted by the solvent dichloromethane in our calculations. Initially, calculations were

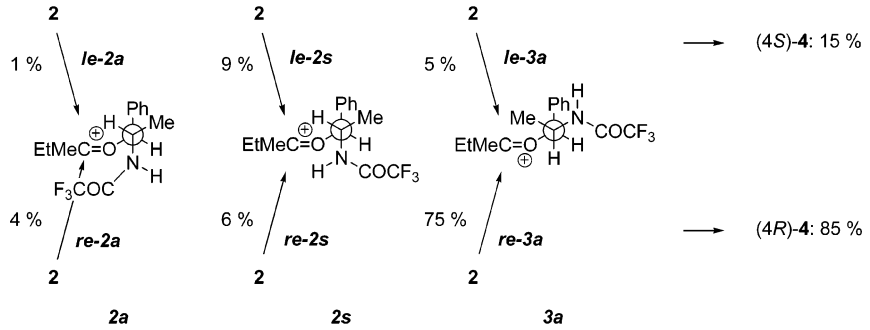

Figure 6. Total contribution of the relevant attack trajectories to the product formation. In each case, the oxocarbenium ion **13** has E configuration. The contribution has been calculated according to the B3LYP-PCM-large//B3LYP-PCM results.

Chart 4. Selected Important TSs As Calculated via B3LYP-PCM[a]

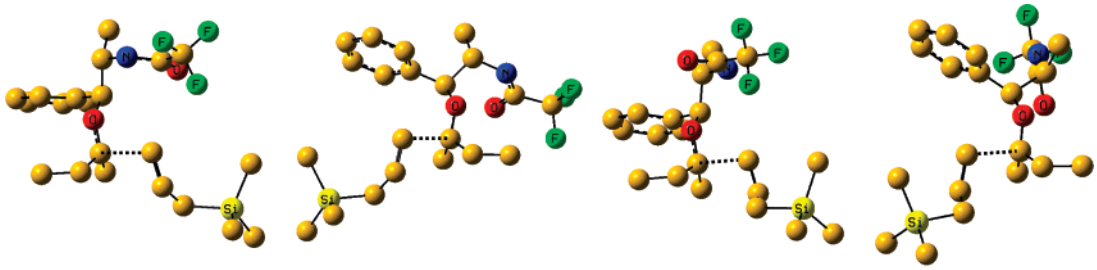

are-b2s ***ale-b2s*** ***dre-b2a*** ***dle-b3a***

[a] Hydrogen atoms are omitted for clarity.

performed with the set of 37 TSs selected from the B3LYP-GP//AM1 approach. Interestingly, and in contrast to our earlier study on related systems,[8] irrelevant TSs from B3LYP-GP calculations became relevant TSs when performing B3LYP-PCM geometry optimizations and frequency calculations. This was mainly the case for TSs with side chain conformations ***2a*** and ***2s***. For this reason, we went back one step and carried out B3LYP-PCM//AM1 single-point calculations for all 264 TSs. By applying a threshold of 12.5 kJ mol^{-1}, 14 additional TSs were selected whose $E_{rel}^{\ddagger}$ values determined by B3LYP-GP//AM1 had been above the gas-phase threshold. For the sake of comparison, these additional TSs for B3LYP-PCM calculations were also included in the B3LYP-GP TS set and were found to remain irrelevant in gas phase.

There are 14 TSs in the region between 0 and 6 kJ mol^{-1}; up to 10 kJ mol^{-1}, this number increases to 30 TSs. Table 2 lists the relevant TSs obtained by B3LYP-PCM and B3LYP-PCM-large//B3LYP-PCM calculations. Because of the exponential weighting of $G_{rel}^{\ddagger}$ via eq 2, the predicted selectivities of 83:17 and 85:15 in comparison to the experimental value of 90:10 indicate that the calculated TS energies $G_{rel}^{\ddagger}$ in solution are much closer to the real $G_{rel}^{\ddagger}$ values than those predicted in gas phase, which yielded a selectivity of 97:3.

Chart 4 illustrates TSs ***are-b2s***, ***ale-b2s***, ***dre-b2a***, and ***dle-b3a*** obtained from B3LYP-PCM calculations. The geometries of TSs ***dre-b3a***, ***are-b3a***, and ***fre-b3a*** are almost identical to those already shown in Chart 3.

According to the B3LYP-PCM results and in line with the B3LYP-GP results, the formation of (4*R*)-**4** can be explained by the attack of **2** to the *Si* face of the E-configured oxocarbenium ion **13**. However, formation of the minor isomer is not predicted to proceed via attack of the corresponding Z-configured ion, but via attack to the opposite face of E-configured **13**. TSs with Z-configured **13** are not among the relevant TSs. However, TSs ***arz-b3a***, ***drz-b3a***, and ***frz-b3a*** have very similar $G_{rel}^{\ddagger}$ values compared to those of B3LYP-GP, but because of the large number of relevant TSs, their contribution to product formation is insignificant.

Table 2. Relevant TSs Obtained via B3LYP-PCM and B3LYP-PCM-large//B3LYP-PCM Calculations

TS[a]	$G_{rel}^{\ddagger}$ (kJ mol^{-1})[b]	c_{TS} (%)[c]		$G_{rel}^{\ddagger}$ (kJ mol^{-1})[d]	c_{TS} (%)	
dre-b3a (*R*)	0.0	33.7		0.0	34.1	
are-b3a (*R*)	0.4	26.8		0.2	30.1	
fre-b3a (*R*)	2.3	8.0		2.4	7.8	
are-b2s (*R*)	3.0	5.2	(4*R*)-**4**:	3.2	4.7	(4*R*)-**4**:
dre-b2a (*R*)	3.2	4.6	83%	3.7	3.5	85%
fre-d3a (*R*)	4.4	2.2		4.0	2.9	
dre-b2s (*R*)	4.8	1.8		5.1	1.5	
are-b2a (*R*)	6.0	0.8		6.5	0.6	
ale-b2s (*S*)	3.0	5.3		3.4	4.2	
dle-b3a (*S*)	3.5	4.0		3.4	4.2	
dle-b2s (*S*)	4.0	2.9	(4*S*)-**4**:	4.3	2.4	(4*S*)-**4**:
ele-b2s (*S*)	4.1	2.6	17%	4.5	2.1	15%
ale-b3a (*S*)	5.4	1.2		5.3	1.3	
ale-b2a (*S*)	5.9	0.9		6.6	0.6	

[a] The induced product stereochemistry at the C-4 position of homoallylic ether **4** is given in parentheses. [b] B3LYP-PCM results. [c] c_{TS} = transition-state contribution, as calculated via eq 2. For the calculation of c_{TS}, only the TSs in the table were considered. [d] B3LYP-PCM-large//B3LYP-PCM results.

Figure 6 illustrates the relevant attack trajectories which lead to the predicted selectivity of 85:15. Limiting the analysis to trajectory ***re-3a*** for the formation of the main isomer and trajectory ***le-2s*** for the formation of the minor isomer results in a correct description of the isomer ratio (89:11); however, such a simplification neglects a number of TSs with a combined contribution of 16% and is therefore not suitable. Thus, the selectivity of the reaction cannot be explained with a simple two-TS model.

In contrast to the B3LYP-GP results, the explanation for the better selectivity with the naphthalene analogue of (*S*)-**6** is now

Table 3. Values of the Geometrical Parameters

	B3LYP-GP					B3LYP-PCM				
TS[a]	$G^{\ddagger}_{rel}$ [b]	*d* (Å)	α (deg)	γ (deg)	δ (deg)	$G^{\ddagger}_{rel}$ [b,c]	*d* (Å)	α (deg)	γ (deg)	δ (deg)
fre-b3a (*R*)	0.0	2.25	105.0	−65.5	84.1	2.4	2.18	104.8	−69.3	84.3
dre-b3a (*R*)	2.8	2.18	98.6	−177.1	96.7	0.0	2.16	98.4	−179.0	91.7
are-b3a (*R*)	3.7	2.19	98.3	−170.2	95.4	0.2	2.15	98.4	−173.6	91.9
fre-d3a (*R*)	4.1	2.29	103.7	−63.2	81.1	4.0	2.21	103.1	−68.6	83.0
bre-b3a (*R*)	6.4	2.25	106.0	66.3	79.9	7.9	2.19	106.2	67.1	80.6
frz-d3a (*S*)	6.6	2.24	103.7	−67.1	84.7	10.8	2.17	104.0	−67.4	85.6
ere-b3a (*R*)	7.1	2.23	107.6	50.9	83.9	6.7	2.17	107.3	55.6	86.4
frz-b3a (*S*)	7.3	2.23	103.8	−76.5	92.5	8.4	2.18	104.0	−76.7	93.5
arz-b3a (*S*)	7.6	2.19	98.6	−179.6	105.0	6.6	2.16	98.6	174.8	104.3
are-d3a (*R*)	9.0	2.22	98.0	−149.6	90.8	13.5	2.16	97.2	−173.6	90.1
drz-b3a (*S*)	9.5	2.18	98.9	179.5	104.8	6.7	2.16	98.7	177.1	103.7
cre-d3a (*R*)	9.6	2.20	108.9	−46.3	78.1	13.8	2.16	108.7	−48.9	78.8
ale-b3a (*S*)	9.9	2.14	98.7	−172.4	131.7	5.3	2.17	98.8	−179.2	112.5
dre-b2a (*R*)	10.8	2.07	100.1	176.1	80.5	3.7	2.11	99.4	176.4	80.7
dle-b3a (*S*)	11.0	2.11	99.5	−179.8	113.2	3.4	2.16	99.0	−179.3	110.4
are-b2s (*R*)	11.2	2.17	99.6	179.6	77.9	3.2	2.14	99.4	177.4	78.5
dre-b2s (*R*)	12.5	2.15	100.0	−177.8	77.2	5.1	2.13	99.7	−178.2	77.7
are-b2a (*R*)	12.8	2.07	100.3	171.0	79.3	6.5	2.10	99.4	176.1	81.0
dle-b2s (*S*)	13.8	2.09	101.1	−178.1	92.6	4.3	2.13	100.7	−175.9	92.4
ale-b2s (*S*)	15.4	2.08	101.2	−172.9	93.4	3.4	2.12	100.7	−174.1	92.0
ele-b2s (*S*)	16.5	2.09	107.7	−65.3	90.7	4.5	2.13	107.4	−65.5	89.9
ale-b2a (*S*)	18.8	2.10	100.8	−173.6	80.5	6.6	2.15	100.6	−172.5	83.4

[a] The induced product stereochemistry at the C-4 position of homoallylic ether **4** is given in parentheses. [b] $G^{\ddagger}_{rel}$ in kJ mol^{-1}. [c] $G^{\ddagger}_{rel}$ obtained from B3LYP-PCM-large//B3LYP-PCM calculations.

straightforward: Attack to the face where the aromatic ring resides is more hindered when the larger naphthalene moiety is used, thus resulting in less formation of the minor isomer and therefore in an overall improved selectivity.

The reduced selectivity with (*S*,*R*)-**3** can now be explained by the same reasoning as before: The $G^{\ddagger}_{rel}$ values of TSs where the silane attacks via trajectory ***re-3a*** increase because the methyl group points toward **2**. On the other hand, the position of the methyl group is less relevant for the attack from the opposite face via trajectory ***le*** which leads to the minor product. Therefore, the selectivity is slightly shifted toward the minor product, leading to a lower selectivity of 87:13 (experimental value).

Replacing the methyl group by a hydrogen atom has a very subtle effect on the selectivity which is slightly decreased from 90:10 to 89:11 in experiment. This can be explained by the somewhat diminished steric hindrance in attack trajectory ***le-3a*** while in all other trajectories, the replacement has no effect. Thus, the corresponding TSs have a lower $G^{\ddagger}_{rel}$ value which results in an overall slightly lower selectivity.

Finally, the higher selectivity with larger methyl ketones can also be easily explained: In TSs with side chain conformations ***2a*** and ***2s***, there is a steric interaction between the ethyl group and the auxiliary's trifluoracetamide group which increases when the ethyl group is replaced by a larger residue. Therefore, TSs with conformation ***3a*** that lack this interaction will become dominant and lead to less formation of the minor isomer.

The fact that the differences in selectivity of similar transformations can be explained with the TS structures in Table 2 strongly indicates that these TSs constitute the correct TSs for the stereoselective allylation of **1** in the presence of (*S*,*S*)-**3**.

Calculated Transition-State Structures. For the inspection of steric interactions, we chose four geometrical parameters of the 22 TSs in Tables 1 and 2. The geometrical parameters, illustrated in Figure 7, comprise the distance between the bond-forming carbon atoms *d*, the Bürgi−Dunitz[18] angle of attack

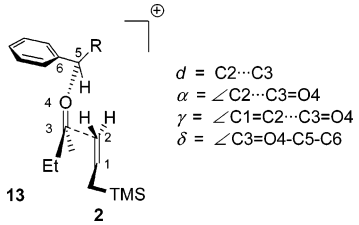

Figure 7. Selected geometrical parameters for the description of TS structures (R = $CH(CH_3)-NHCOCF_3$).

α, the torsional angle γ that is a measure for the relative orientation of the double bonds in **2** and **13**, and the torsional angle δ that indicates the position of the chiral auxiliary. Table 3 lists the values for the chosen parameters for TS geometries found by B3LYP-GP and B3LYP-PCM geometry optimizations.

Rationalization of Gas-Phase Transition-State Energies. The influence of steric and electronic effects can best be derived from gas-phase $G^{\ddagger}_{rel}$ values since energy differences in solution include the free energy of solvation ΔG_{solv} as an additional contribution. Without solvent, it is obvious that auxiliary side chain conformation ***3a*** is strongly favored over other conformations. In this conformation, maximum distance between the silane **2** and the trifluoroacetamide group as well as methyl group of the auxiliary ensures minimum unfavorable steric interactions and therefore lowest $G^{\ddagger}_{rel}$ value, when **2** approaches via trajectories ***re*** or ***rz***. In contrast, attack from the opposite face is very unfavorable, as can be seen from the $G^{\ddagger}_{rel}$ values of TSs ***ale-b3a*** and ***dle-b3a***. In these TSs, the phenyl group needs to tilt away from the approaching allyl silane (δ = 130° and 113°, respectively), resulting in a loss of electronic stabilization of the ionic species.

Almost identical parameters are found for TSs ***fre-b3a***, ***fre-d3a***, ***frz-d3a***, and ***frz-b3a***. From this observation we conclude that energy differences between these TSs can solely be traced back to energy differences between E- and Z-configured **13** and between the two possible ethyl group conformations. As expected, E-configured **13** is more stable than the Z-configured counterpart. Steric interactions are limited when the ethyl group points away from the approaching silane unless this would introduce an increase in interaction between the ethyl group

(18) Bürgi, H.; Dunitz, J. D.; Shepter, E. *J. Am. Chem. Soc.* **1973**, *95*, 5065−5067.

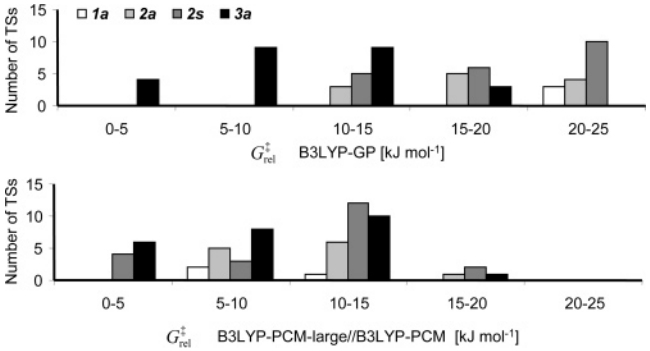

Figure 8. Number of TSs, grouped by side chain conformations ***1a***, ***2a***, ***2s***, and ***3a***, depending on $G^{\ddagger}_{rel}$ range. The figure comprises all 61 preselected TSs.

and the phenyl group. This simple reasoning explains the order of $G^{\ddagger}_{rel}$ for TSs which does not differ in the remaining four conformational degrees of freedom.

Finally, TSs with $\gamma \approx 180°$ (TSs starting with ***a*** or ***d***) are generally most favorable in terms of steric interactions of **2** with the chiral auxiliary. On the other hand, the Bürgi−Dunitz angle α in these TSs is only about 100° as opposed to the idealized value of 107° which, however, can be achieved in TSs with $\gamma \approx +60°$ and $\gamma \approx -60°$ (TSs starting with ***b***, ***c***, ***e,*** and ***f***).

To summarize, the gas-phase $G^{\ddagger}_{rel}$ values can be rationalized by the following effects: (1) Side chain conformation ***3a*** is most favorable because of minimum steric interactions; (2) attack occurs preferentially to the face opposite the phenyl group (trajectories ***re*** and ***rz***); (3) E-configured **13** is more stable than Z-configured **13**; (4) a stereoelectronic effect stabilizes conformations with $\delta \approx 90°$; (5) the ethyl group should point away from the approaching silane (conformation ***b*** vs ***d***); (6) a Bürgi−Dunitz angle α of 107° is favored (TSs starting with ***b***, ***c***, ***e***, and ***f***); and (7) minimum steric interactions between the CH_2-TMS group of the silane with the auxiliary side chain lead to low-energy TSs (TSs starting with ***a*** and ***d***).

Thus, TS ***fre-b3a*** is the lowest-energy TS since all criteria but the last one are met. Following are TSs ***dre-b3a*** and ***are-b3a*** where there is no interaction between the CH_2TMS group of **2** and the auxiliary side chain but where α is only about 100°. In consequence to the listed criteria, the minor isomer (4*S*)-**4** may only be formed by attack to the Z-configured ion **13**.

Rationalization of Transition-State Energies in Dichloromethane Solution. Inspection of Table 3 reveals that TS geometries obtained in gas phase and in solution are almost identical. The nevertheless large difference between $G^{\ddagger}_{rel}$ values from B3LYP-GP and B3LYP-PCM calculations must therefore be traced back to largely divergent free energies of solvation, ΔG_{solv}.

Figure 8 illustrates the change of $G^{\ddagger}_{rel}$ of TSs with side chain conformations other than ***3a*** when going from gas phase to dichloromethane solution. (TSs with conformations ***1s*** and ***3s*** were not selected for the set of 61 TSs.)

While the relative energies between TSs with the same side chain conformation remain approximately the same, the complete subsets of TSs with conformations ***2a***, ***2s,*** and ***1a*** are shifted to lower energies. To quantify this effect, we have determined ΔG_{solv} values for all TSs by comparison of single-point B3LYP-GP//B3LYP-PCM energies with direct B3LYP-PCM energies (Table 4).

Table 4. Free Energy of Solvation ΔG_{solv}, Grouped by Side Chain Conformation

side chain conformation	no. of TSs	ΔG_{solv}[a] (kJ mol^{-1})	$\Delta G_{solv,\,rel}$[b] (kJ mol^{-1})	SD[c] (kJ mol^{-1})
1a	3	−145.0	−17.6	0.7
2a	12	−137.2	−9.7	2.5
2s	21	−134.7	−7.2	2.5
3a	25	−127.5	0.0	3.1

[a] ΔG_{solv} mean value over all TSs with the given conformation. [b] Relative ΔG_{solv} mean value with $\Delta G_{solv,\,rel}$ (***3a***) set to 0 kJ mol^{-1}. [c] Standard deviation of ΔG_{solv} over all TSs with the given conformation.

In relation to TSs with conformation ***3a***, those with conformation ***2s*** become energetically more accessible by more than 7 kJ mol^{-1}; for conformations ***2a*** and ***1a*** this value is even larger. But as this gain of relevance is not sufficient to replace ***3a*** TSs as the most relevant TSs, the number of relevant TSs increases dramatically.

Two factors have a large impact on free energies of solution: the solvent accessible surface and dipole moment of the solute. The dipole moments lie between 9 and 10 D (calculated with B3LYP-PCM-large//B3LYP-PCM) for TSs with conformations ***2a***, ***2s,*** and ***3a*** without significant differences among the conformations. In contrast, ***1a*** TSs have a dipole moment of larger than 15 D which might explain the very large ΔG_{solv} value in comparison to the other conformations.

TSs with conformation ***2s*** and ***2a*** are much more "compact" than their ***3a*** counterparts. This fact is nicely observable by inspection of Charts 2−4. This "compactness" adds steric interactions within the TS, which is why such TSs play no role in the gas phase. However, this effect is counterbalanced by the strongly increased free energy of solvation in the noncoordinating solvent dichloromethane.

Activation Energy. For the determination of the activation energy of the stereogenic step in solution, the ground-state geometries for oxocarbenium ion **13** and silane **2** were identified with B3LYP-PCM. The difference of the free energy values of TS ***dre-b3a*** and of the sum of the free energies of **2** and **13**, all obtained from B3LYP-PCM-large//B3LYP-PCM calculations, were interpreted as activation energy $\Delta G^{\ddagger}$ which was determined to be 139.1 kJ mol^{-1}.

5. Conclusion

The multicomponent domino reactions of aliphatic methyl ketones, allyltrimethylsilane, and a chiral norpseudoephedrine-derived silyl ether auxiliary lead to homoallylic ethers with excellent induced diastereoselectivity. In this study, we have identified the relevant TSs of the stereogenic step of the multicomponent allylation of **1** both in gas phase and in dichloromethane solution. The energy differences of the TSs from calculations in solution predict a selectivity of 85:15 while the experimental value is 90:10. In gas-phase calculations, a selectivity of 97:3 was found. As the stereogenic step, the addition of **2** to an intermediate oxocarbenium ion from **1** and the silyl ether was assumed.

Because of the large number of possible TSs (almost 300), a screening process was developed and validated which allowed the selection of a subset that contains all important TSs. Thus, 61 TSs were subject to DFT calculations in the gas phase and in dichloromethane solution. We found that relative energies differ significantly when going from the gas phase to solution.

The influence of steric and electronic effects on the relative energy was extracted from gas-phase results while the changes when going from gas phase to solution could be traced back to different values for the free energy of solution for certain sets of TSs.

It is not possible to explain the selectivity of the reaction with a simple two-transition-state model. Instead, more than 10 TSs contribute significantly to product formation. However, the high selectivity can be traced back to three side chain conformations which allow different faces of the oxocarbenium ion to be attacked. With the obtained results, the rationalization of divergent selectivities with analogues of the chiral auxiliary as well as increased selectivities for larger methyl ketones is straightforward.

We wish to point out that limiting this study to gas-phase results (even with single-point calculations in solvent on relevant gas-phase TSs) would have led to different conclusions about the relevant TSs and the origin of the minor isomer.

Acknowledgment. This work has been supported by the Fonds der Chemischen Industrie. We thank the Gesellschaft für wissenschaftliche Datenverarbeitung Göttingen (GWDG) for providing access to their computing resources. T.K. acknowledges the Studienstiftung des deutschen Volkes for a Ph.D scholarship.

Supporting Information Available: Complete ref 14; table of B3LYP//AM1 results for 264 TSs; tables of absolute energies, $G^{\ddagger}_{rel}$, and c_{TS} for the set of 61 TSs in gas phase and in dichloromethane solution; and Cartesian coordinates for the relevant TSs in gas phase and in dichloromethane solution. This material is available free of charge via the Internet at http://pubs.acs.org.

JA078032A